

Strain-Tuned Magnetic Frustration in a Square Lattice J_1 - J_2 Material

I. Bialo,^{1, 2, *} L. Martinelli,¹ G. De Luca,³ P. Worm,⁴ A. Drewanowski,¹ J. Choi,⁵ M. Garcia-Fernandez,⁵ S. Agrestini,⁵ Ke-Jin Zhou,⁵ L. Guo,⁶ C. B. Eom,⁶ J. M. Tomczak,^{7, 4} K. Held,⁴ M. Gibert,⁴ Qisi Wang,^{8, 1, †} and J. Chang¹

¹Physik-Institut, Universität Zürich, Winterthurerstrasse 190, CH-8057 Zürich, Switzerland

²AGH University of Science and Technology, Faculty of Physics and Applied Computer Science, 30-059 Kraków, Poland

³Institut de Ciència de Materials de Barcelona (ICMAB-CSIC), 08193 Bellaterra (Barcelona), Spain

⁴Institute of Solid State Physics, Vienna University of Technology, A-1040 Vienna, Austria

⁵Diamond Light Source, Harwell Campus, Didcot, Oxfordshire OX11 0DE, United Kingdom

⁶Department of Materials Science and Engineering,

University of Wisconsin-Madison, Madison, 53706, Wisconsin, USA

⁷Department of Physics, King's College London, Strand, London WC2R 2LS, United Kingdom

⁸Department of Physics, The Chinese University of Hong Kong, Shatin, Hong Kong, China

(Dated: June 12, 2023)

Magnetic frustration is a route that can lead to the emergence of novel ground states, including spin liquids and spin ices. Such frustration can be introduced through either the geometry of lattice structures or by incompatible exchange interactions. Identifying suitable strategies to control the degree of magnetic frustration in real systems is an active field of research. In this study, we devise a design principle for the tuning of frustrated magnetism on the square lattice through the manipulation of nearest (NN) and next-nearest neighbor (NNN) antiferromagnetic (AF) exchange interactions. By studying the magnon excitations in epitaxially-strained La_2NiO_4 films using resonant inelastic x-ray scattering (RIXS) we show that, in contrast to the cuprates, the dispersion peaks at the AF zone boundary. This indicates the presence of an AF-NNN spin interaction. Using first principles simulations and an effective spin-model, we demonstrate the AF-NNN coupling to be a consequence of the two-orbital nature of La_2NiO_4 . Our results demonstrate that compressive strain can enhance this coupling, providing a design principle for the tunability of frustrated magnetism on a square lattice.

The square-lattice Heisenberg model is the subject of intense numerical and experimental investigations. In spin-1/2 systems—such as cuprates [1] and copper deuteroformate tetradeurate (CFTD) [2]—higher-order exchange interactions are inferred from observations of magnon dispersions along the magnetic zone boundary [3, 4]. While a detailed magnon characterization is useful to understand quantum fluctuation effects, magnetic frustration is typically avoided in these systems. Indeed, the antiferromagnetic (AF) nearest-neighbour (NN) exchange interaction ($J_1 > 0$) and the ferromagnetic next-nearest-neighbour (NNN) interaction ($J_2 < 0$)

stabilize a classical AF Néel order. Instead, magnetic frustration requires both $J_1 > 0$ and $J_2 > 0$. This exchange-frustrated regime of the J_1 - J_2 model is the subject of extensive computational investigations for both spin $S = 1/2$ [5–9] and $S = 1$ [10, 11] systems. In a narrow range near $J_2/J_1 \sim 1/2$, magnetic frustration is found to dominate and may lead to exotic quantum phases such as the spin-liquid state [12], which yet lacks experimental observation. Several calculations show that the Néel order is destroyed there and the ground state has a valence-bond character [12–14], although its exact nature is still subject of debate [7, 15]. However, only very few square-lattice systems exhibit substantial magnetic frustration [16, 17], and even fewer display tunable magnetic interactions [18]. As a result, approaching the interesting parameter regime in real materials remains an ongoing issue.

The continuously improving energy resolution of resonant inelastic x-ray scattering (RIXS) [19] brings new opportunities. Higher-order magnetic exchange interactions have been measured with exquisite precision [20] and, more recently, momentum-dependent electron-phonon couplings [21] have been extracted from experiments. As RIXS experiments are compatible with thin films, simultaneous tuning and probing of magnetic interactions has become possible.

In this article, we provide a high-resolution RIXS study of magnetic excitations in La_2NiO_4 thin films (LNO) on different substrates. We discover a marked, upward dispersion along the AF zone-boundary $(1/2, 0) \rightarrow (1/4, 1/4)$, which reveals the presence of strong, AF-NNN interactions that frustrate the NN one. By employing *ab initio* calculations, we demonstrate that these results can only be explained by including the multi-orbital nature of $3d^8$ -Ni systems. More interestingly, we observe a correlation between the relative strength of the magnetic interactions and the strain applied onto the films. Our results demonstrate that 214-type nickelates are a promising class of materials for the study of the AF, square-lattice Heisenberg model. Moreover, the use of thin films provides a clear route to tune the magnetic frustration and explore

* izabela.bialo@uzh.ch

† qwang@cuhk.edu.hk

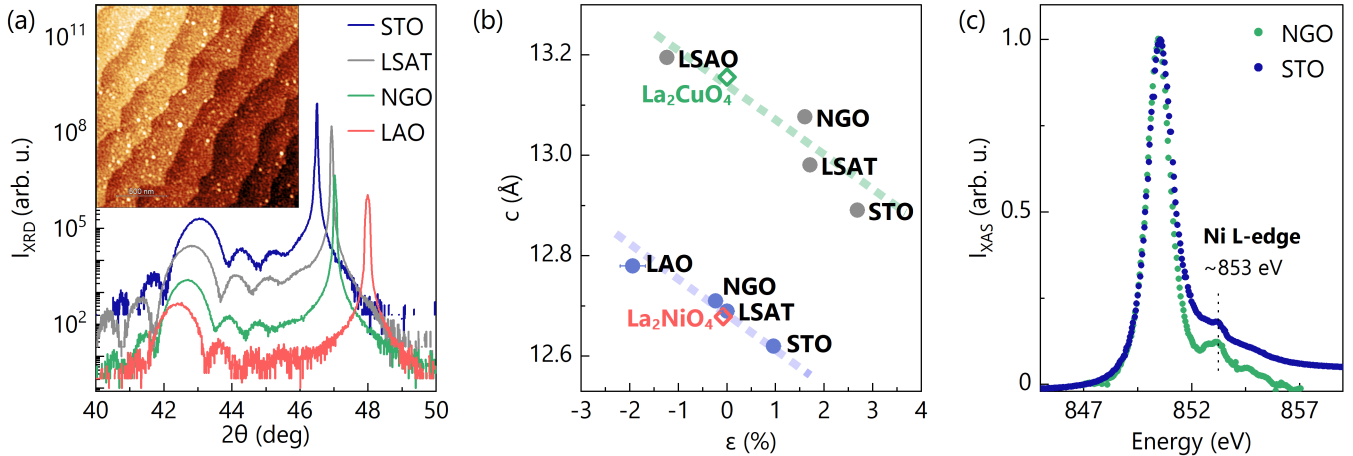


FIG. 1. **Characterization measurements on thin films of La₂NiO₄.** (a) X-ray diffraction (at 300 K) probing the (0, 0, ℓ) direction of 12 nm thin films of La₂NiO₄ on substrates as indicated. The inset represents the atomic force microscopy image showing the step-like morphology of the films (here for the NGO substrate). The color scale corresponds to the film thickness. (b) c -axis lattice parameter versus in-plane epitaxial strain (at 300 K) calculated for LNO (purple dots) and La₂CuO₄ [22] (gray dots) films grown on different substrates as a relative change of in-plane parameters in reference to bulk (diamonds) with $a = 3.868$ Å and $c = 12.679$ Å for an isomorphous La₂NiO₄ [23] and $a = 3.803$ Å and $c = 13.156$ Å for La₂CuO₄ [24]. (c) X-ray absorption spectra around the Ni L -edge. The dominant peak corresponds to the La M -edge. (b,c) Dashed lines are guides to the eye.

so far inaccessible regions of the magnetic phase diagram.

Results

Our thin films of La₂NiO₄ on SrTiO₃ (STO), LaAlO₃ (LAO), (LaAlO₃)_{0.3}(Sr₂TaAlO₆)_{0.7} (LSAT) and NdGaO₃ (NGO) substrates are characterized by atomic force microscopy (AFM), x-ray diffraction (XRD), and x-ray absorption spectroscopy (XAS) – see Fig. 1. The AFM images display a step-like morphology indicating an excellent layer-by-layer growth. Diffraction patterns probing the (0, 0, ℓ) reciprocal direction demonstrate good single crystallinity and allow us to extract the c -axis lattice parameters of the films. The epitaxial strain applied by the substrates is supported by the film c -axis and in-plane lattice parameter dependence (Fig. 1b). The XAS spectra recorded on the LNO/STO and LNO/NGO are consistent with what is observed on related nickelates [25–27].

The RIXS spectra of LNO films were measured at the Ni L_3 edge (853 eV). These spectra exhibit key RIXS excitations, including high-energy dd -excitations (approximately 0.5–3 eV), an elastic scattering contribution at 0 eV, as well as phonon and magnon excitations in between. The dd -excitations have a multi-peak structure, qualitatively similar to other 3d⁸ systems as NiO [25–28]. As shown in Figs. 2a, the relative intensities of the peaks are different in the three samples, due to the different crystal fields acting on the Ni atoms. The subtraction of the elastic peak clearly highlights the presence of multiple low-energy features; see Figs. 2b,c.

To extract the dispersion of magnetic excitations, we assumed a two-mode model with the addition of a high-

energy continuum “background” (Fig. 2b,c). Each of these components is represented by a Gaussian. This provides an effective fitting model of excitations for all measured film systems and momenta. Our interpretation of the proposed model is based on the hypothesis that the lower-energy mode (~40 meV) stems from an optical phonon, while the higher-energy mode (strongly dispersing between 60 and 120 meV) is a magnon. This assignment is supported by previous neutron scattering measurements that identified the phonon part via an out-of-plane oxygen buckling mode [29, 30]. The interpretation of the higher-energy mode as a magnon is consistent with earlier RIXS [31] and neutron studies [32] of bulk La₂NiO₄. The resulting magnon dispersions are shown in Fig. 3.

Due to lower energy resolution, the previous RIXS study [31] did not resolve any phonon excitations. The unresolved phonon excitation implied that the phonon and magnon spectral weights were merged. This in turn influences the extraction of the magnon dispersion. Having access, in this work, to a higher energy resolution, we can distinguish between the nearly momentum-independent phonon mode and the dispersive magnon branch along the three measured high-symmetry directions. In all film systems explored, the magnon energy reaches its maximum at the AF zone boundary, at the Σ point (1/4, 1/4), referred to as E_{Σ} , while it displays a local minimum at the X point (1/2, 0), referred to as E_X . Until recently [33], this evidently anisotropic shape of the magnon dispersion had not been reported in earlier studies [31, 32]. Furthermore, the energy E_{Σ} is different for all three substrates. In

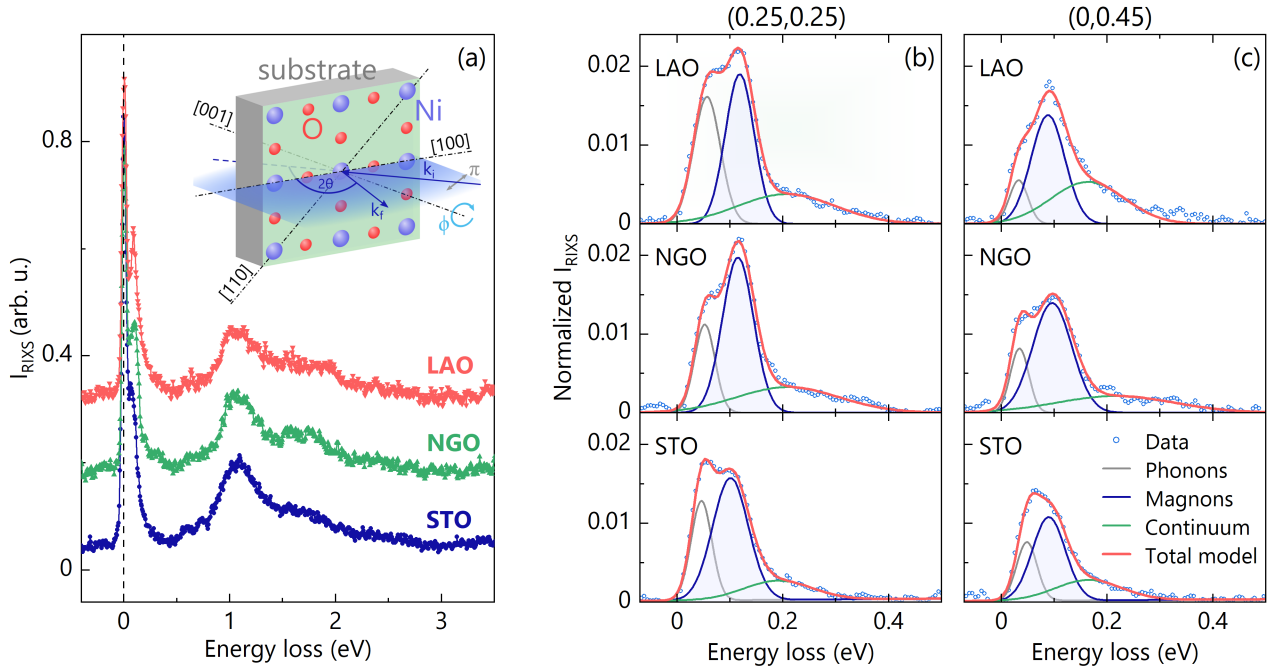


FIG. 2. **Resonant inelastic x-ray scattering spectra of LNO.** (a) Raw spectra recorded in LNO films with substrates as indicated. (a,inset) Schematics of the photon-in-photon-out RIXS geometry with horizontally polarized light (π) and azimuthal sample rotation angle ϕ . (c,d) Low-energy part of the RIXS spectra with momentum transfer and film substrates indicated. The solid red line indicates a three-component fit (see text) with phonon, magnon (shaded), and multi-magnon (continuum) contributions. The elastic scattering channel is subtracted in (b,c).

particular, it increases as a function of compressive strain, with an enhancement of 18 ± 4 meV ($\sim 20\%$) from LNO/STO to LNO/LAO.

Discussion

By resolving both the phonon and magnon modes, we find that the zone boundary magnons display a non-negligible dispersion. The direct implication is the presence of higher-order effective magnetic exchange interactions. In La_2CuO_4 and related Mott insulating cuprates, the zone boundary dispersion has been interpreted in terms of a positive ring-exchange interaction that emerges naturally from a *single-orbital* Hubbard model [22, 34, 35]. There is, however, an important difference between the zone-boundary dispersion of La_2CuO_4 and La_2NiO_4 : in contrast to La_2CuO_4 , the zone boundary dispersion of La_2NiO_4 has its maximum at the AF zone boundary Σ point rather than at the X point. As such, the magnon dispersion of La_2NiO_4 cannot be described from a single band Hubbard model—at least not in the strong coupling limit where the projection onto a Heisenberg spin Hamiltonian is viable.

As a first step, we parameterize the magnon dispersion of LNO using a phenomenological spin-wave model that includes effective NN and NNN exchange interactions, respectively J_1 and J_2 (Fig. 3), plus an easy-plane anisotropy K , already reported by previous measurements [32, 33]. As a starting point we employ the

AF structure of bulk La_2NiO_4 determined by neutron diffraction [36–38], with the spin direction parallel to the crystallographic a -axis. The model is solved in a linear spin wave (large- S) limit, and the calculated dispersion is fitted to the measured one (see Methods). Fitting the experimental (“exp”) data yields an effective NN exchange interaction $J_1^{\text{exp}} \sim 30$ meV consistent with previous neutron and RIXS results [31, 39]. Due to the demonstrated finite zone boundary dispersion, our spin-wave model fitting also yields a moderate NNN exchange interaction J_2^{exp} . Importantly, J_2^{exp} is *positive* and enhanced by compressive strain [3, 4]. In what follows, we wish to extract the frustration parameter $\mathcal{G} = J_2^{\text{exp}}/J_1^{\text{exp}}$ with the highest precision. Within our spin-wave model, $E_X = 4SZ_c(J_1 - 2J_2)$ and $E_\Sigma = 4SZ_c(J_1 - J_2)$, where Z_c is the quantum renormalization factor for spin wave energies, which is taken as $Z_c = 1.09$ [40]. This gives $\mathcal{G}^{-1} = 1 + E_\Sigma/(E_\Sigma - E_X)$. The frustration parameter \mathcal{G} is thus derived directly from experimental data and plotted as a function of c lattice parameter in Fig. 4. Due to the Poisson effect, the c lattice parameter undergoes proportional shrinkage when in-plane parameters expand. Our XRD measurements confirm this relationship (Fig. 1b), indicating that the c lattice parameter can serve as a direct probe of the in-plane strain. Thus, our findings demonstrate a nearly linear correlation between magnetic frustrations and epitaxial strain.

We stress that, for interaction strengths and hoppings

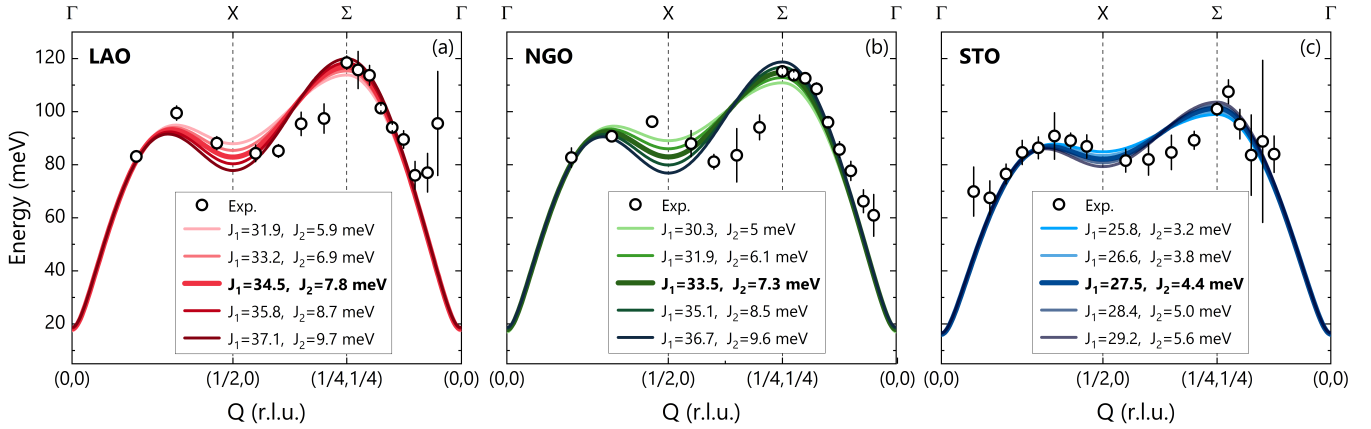


FIG. 3. **Magnon dispersion of La₂NiO₄ films.** (a-c) Magnon excitation energies (open dots) along high symmetry directions for La₂NiO₄ on substrates as indicated. Solid lines represent the same spin wave model (see text) evaluated for different exchange parameters within the confidence intervals of the fitted parameters. The curves corresponding to the best-fit values (marked with bold in the legend) are reported as thicker lines. The middle segment, X → Σ, is part of the AF zone-boundary. Error bars are determined from the fitting uncertainty.

that are realistic for cuprates and nickelates, $J_2 > 0$ is hard to reconcile with a single-band Hubbard model. A positive J_2 implies an effective AF NNN exchange interaction, at odds with what is observed in cuprates [4, 34] and d^9 infinite-layer nickelates [41, 42]. Both systems have indeed been successfully described using a single d -orbital framework [3, 4, 43, 44]. Therefore, we argue that the magnon zone boundary dispersion in La₂NiO₄ signals physics beyond the single-orbital Hubbard model. We propose that the multi-orbital ($d_{x^2-y^2}$, d_{z^2}) nature of nickelates [45–47] must be explicitly considered. Already in La₂CuO₄, due to the short apical oxygen distance, small but significant orbital hybridization d_{z^2} and $d_{x^2-y^2}$ has been reported [48]. In La₂NiO₄ the apical oxygen distance is even shorter, as exemplified by the reduced c lattice parameter (see Fig. 1b), and hence an even more pronounced hybridization is expected.

To rationalize the trend in the exchange interactions obtained from our spin-wave fits, we derive a two-orbital low-energy model for La₂NiO₄ on different substrates from first principles (see the Method section). For the Ni d_{z^2} and $d_{x^2-y^2}$ orbitals (labeled “α” and “β”), we compute the (next) nearest-neighbor hopping parameters $t^{(i)}$, the crystal field splitting $Δ$, local Coulomb (Hubbard) interaction U and Hund’s exchange J_H using experimental lattice constants from Table I. Noteworthy[49], the hopping parameters and Coulomb interactions, listed in Table I, hardly change under varying in-plane compression. This is different from calculations for the cuprate family, see Ref. 22, and agrees with our experiments, which show substantially smaller changes in the magnon spectrum than for the cuprates. What is most affected by strain in Table I is the crystal field splitting $Δ$ by which the Ni $d_{x^2-y^2}$ orbital is higher in energy than the d_{z^2} orbital. When going from the STO to the LAO substrate,

in-plane strain pushes the $d_{x^2-y^2}$ orbital further up in energy, as it is pointing towards the now closer in-plane oxygen sites that are charged negatively.

This crystal-field splitting enters the calculated (“cal”) two-orbital superexchange as follows:

$$J_1^{\text{cal}} = \frac{t_{\alpha\beta}^2}{U + J_H - \Delta} + \frac{t_{\alpha\beta}^2}{U + J_H + \Delta} + \frac{t_{\alpha\alpha}^2 + t_{\beta\beta}^2}{U + J_H}, \quad (1)$$

where we extend the formula of Ref. 50 to finite $Δ$. As $Δ$ appears once with a plus and once with a minus sign in the denominator, the crystal-field splitting enters J_1^{cal} in a higher-than-linear order.

The magnetic exchange couplings J_1^{cal} determined by Eq. (1) are displayed in Table I. They show the same qualitative tendency as in our experiment, i.e., an increase of both J_1^{exp} (see Fig. 3) and J_1^{cal} with compressive strain. Quantitatively, the *ab initio* calculated J_1^{cal} is however notably too large. This has two origins: (i) The cRPA interactions are, here, taken at zero frequency $U = U(\omega = 0)$. Additional renormalizations from the frequency dependence $U(\omega)$ [51] are often mimicked through an empirical enhancement of U . (ii) Eq. (1) only includes terms to second-order perturbation theory in t . For the one-band Hubbard model, higher-order processes have been calculated and yield a correction from $J_1 = 4t^2/U$ to a reduced $J_1 = 4(t^2/U - 16t^4/U^3)$ [43, 52]. Higher order terms are expected to reduce J_1 also in the two-orbital setting. Here, we estimate these corrections by the one-orbital prescription $t^2/U \rightarrow t^2/U - 16t^4/U^3$. Then, e.g., for the NGO substrate, the leading contribution to J_1^{cal} , i.e., $t_{\beta\beta}^2/(U_{\text{eff}})$ with $U_{\text{eff}} = U + J_H$, reduces from 47 meV to 37 meV. Applying this substitution to Eq. (1) yields the corrected exchange couplings $J_1^{\text{cal,corr}}$ listed in Tab. I, which are in better agreement with the measured values (see Fig. 3).

System	a [Å]	c [Å]	Δ [eV]	$t_{\alpha\alpha}$ [eV]	$t_{\beta\beta}$ [eV]	$t_{\alpha\beta}$ [eV]	$t'_{\alpha\alpha}$ [meV]	$t'_{\beta\beta}$ [meV]	$U_{\alpha\alpha}$ [eV]	$U_{\beta\beta}$ [eV]	$U_{\alpha\beta}$ [eV]	J_H [eV]	J_1^{cal} [meV]	J_2^{cal} [meV]	$J_1^{\text{cal,corr}}$ [meV]
La ₂ NiO ₄	3.890	12.55	0.48	-0.070	-0.403	-0.161	-9	75	3.06	3.15	1.97	0.52	61	1.57	51
LNO/STO	3.905	12.62	0.48	-0.067	-0.395	-0.156	-8	74	3.01	3.14	1.94	0.52	58	1.56	50
LNO/NGO	3.859	12.71	0.58	-0.064	-0.414	-0.155	-7	77	3.03	3.16	1.97	0.51	62	1.64	52
LNO/LAO	3.793	12.78	0.74	-0.060	-0.447	-0.156	-6	80	3.02	3.07	1.93	0.50	72	1.83	57

TABLE I. Crystal field splitting Δ , (next-)nearest neighbor hopping $t_{ij}^{(i)}$ between i -th and j -th Ni orbitals (α and β here denote the z^2 and $x^2 - y^2$ orbital, respectively), the inter- and intra-orbital Coulomb interaction U_{ij} , and Hund's exchange J_H between the two orbital as calculated by DFT and cRPA with the in-plane lattice constant a of the three substrates; note that $t'_{\alpha\beta} = 0$ by symmetry. From these *ab initio* calculated parameters the spin couplings J_1 and J_2 are determined as the super-exchange from second order perturbation theory using Eq. (1). Estimating higher order terms using a one-orbital analogy, yields the reduced $J_1^{\text{cal,corr}}$ couplings – see text. The bulk lattice parameters refer to the low temperature tetragonal polymorph of La₂NiO₄, after Ref. 33.

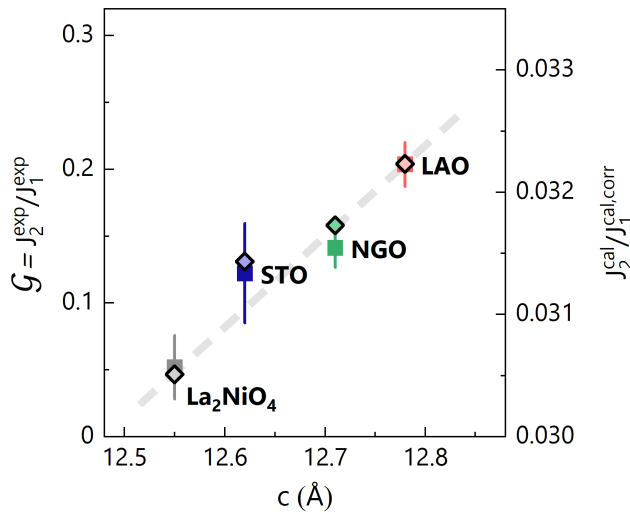


FIG. 4. **Strain dependent magnetic frustration.** The frustration parameter $\mathcal{G} = J_2^{\text{exp}}/J_1^{\text{exp}}$ derived from the experimental data (squares; left axis) is presented as a function of the c -axis lattice parameter. Error bars for the experimental data are calculated as a propagation of standard deviations extracted from the fits. The results for films are combined with data for bulk La₂NiO₄ from Ref. 33. The experimental frustration \mathcal{G} is compared to the ratio $J_2^{\text{cal}}/J_1^{\text{cal,corr}}$ derived from the DFT and cRPA calculations (diamonds; right axis). Note that the calculated J_2^{cal} only contains a *contribution* to the full next nearest-neighbor coupling J_2 . Therefore, the comparison merely highlights a similar *trend* of the frustration under in-plane compression. The dashed line is a guide-to-the-eye.

Table I also lists the next-nearest neighbor exchange J_2^{cal} that can be obtained with the same second-order formula Eq. (1), except now using the hoppings t' instead of t . Crucially, our calculations predict a positive J_2 , in agreement with the experiment. Moreover, J_2^{cal} shows the same qualitative tendency as in the experiment as a function of epitaxial strain. On a quantitative level, the calculated values are, however, a factor $\sim 3 - 5$ lower than the experimental results. The reason is that contributions to J_2 from higher-order exchange processes,

of order t^4/U^3 and $t't^2/U^2$, become (relatively) more important for J_2^{cal} , as the second-order terms are now based on the much smaller t' .

The key difference between the *multi-orbital* case of LNO and the *one-orbital* cuprates is the larger U ($U_{\text{cRPA}} \approx 3.1$ eV for two-orbitals while $U_{\text{cRPA}} \approx 1.9$ eV for a one Ni $d_{x^2-y^2}$ orbital setup) and the additional Hund's $J_H \approx 0.5$ eV in the denominator of Eq. (1). As a consequence, the balance for the NNN exchange coupling shifts from a *ferromagnetic* ring exchange $J_2 \sim -t^4/U_{\text{eff}}^3 < 0$, that overpowers the *AF* second-order exchange $J_2 \sim t'^2/U_{\text{eff}} > 0$ in the one-orbital cuprates, toward dominance of the latter in the multi-orbital LNO. This change in hierarchy explains the main qualitative differences in magnon dispersion between LNO and cuprates: the opposite sign of the effective J_2 . For LNO, with a positive J_2 , the zone-boundary dispersion shows a notable minimum at $(1/2, 0)$, see Fig. 3, whereas a maximum occurs for the negative J_2 in cuprates.

The *ab-initio* calculations indicate that the magnetic frustration is caused by the multi-orbital nature of 3d⁸ nickelates. More importantly, our results demonstrate that the degree of frustration is amplified by compressive strain (see Fig. 4), with a pivotal role played by the crystal-field splitting. Indeed, with the substrates used, the magnetic frustration increases four-fold with respect to the bulk, bridging half the way toward the exotic realm anticipated for $J_2/J_1 \sim 1/2$. Thus, our study provides a design principle and experimental pathway for investigating the impact of frustration on the magnetic ground state of a J_1 - J_2 square lattice, addressing a long-standing open question. It highlights that epitaxial strain can offer a powerful experimental route to reach so far unexplored regions of the magnetic phase diagram, potentially allowing to investigate exotic states induced by magnetic frustration.

Methods

Film growth and characterization. Thin films of La₂NiO₄ were grown by RHEED-equipped Radio-Frequency off-axis magnetron sputtering [53] on (001) SrTiO₃ (STO), (001) LaAlO₃ (LAO), (001)

$(\text{LaAlO}_3)_{0.3}(\text{Sr}_2\text{TaAlO}_6)_{0.7}$ (LSAT) and (110) NdGaO_3 (NGO) substrates. These films were grown in an argon atmosphere at 700°C. Their qualities were confirmed by AFM and XRD.

RIXS experiments. Ni L -edge RIXS experiments were carried out at the I21 beamline [54] at the DIAMOND Light Source. All spectra were collected in the grazing exit geometry using linear horizontal polarized incident light with the scattering angle fixed to $2\theta = 154^\circ$. The energy resolution, estimated from the elastic scattering on amorphous carbon tape, was between 37-41 meV (full-width-at-half-maximum, FWHM). All films were measured at base temperature $T = 16$ K. We define the reciprocal space (q_x, q_y, q_z) in reciprocal lattice units $(h, k, \ell) = (q_x a/2\pi, q_y b/2\pi, q_z c/2\pi)$ where a, b and c are the pseudo-tetragonal lattice parameters. RIXS intensities are normalized to the weight of the dd excitations.

Phenomenological spin-wave model. The effective superexchange parameters were extracted from the measured dispersion using a linear spin wave model. We included effective couplings between first and second nearest neighbours, plus an easy-plane anisotropy K , with a resulting Hamiltonian:

$$\mathcal{H} = J_1 \sum_{\langle i,j \rangle} \mathbf{S}_i \cdot \mathbf{S}_j + J_2 \sum_{\langle\langle i,j \rangle\rangle} \mathbf{S}_i \cdot \mathbf{S}_j + K \sum_i (S_i^z)^2 \quad (2)$$

where $\langle i, j \rangle$ and $\langle\langle i, j \rangle\rangle$ denote pairs of first and second nearest neighbours Ni atoms, respectively. The fitting procedure has been carried out using the SpinW package [55]. As an input we have used the AF structure of the bulk La_2NiO_4 determined by neutron diffraction [36–38], with the spin direction parallel to the crystallographic a -axis. The quantum renormalization factor for spin-wave velocity is fixed to $Z_c = 1.09$, as usual for $S = 1$ systems [40]. The value of the easy-plane anisotropy K mostly controls the size of the magnon gap at the Γ point. Since this value is very hard to obtain from RIXS spectra, we have fixed $K = 0.5$ meV in agreement with previous inelastic neutron scattering data [32]. We have also neglected other interactions $< 10^{-1}$ meV such as easy-axis anisotropy, inter-layer coupling and Dzyaloshinskii–Moriya interactions [33, 37].

***Ab initio* calculations.** Electronic structure calculations were performed with the density functional theory in the local density approximation using a full-potential linearized muffin-tin orbital code [56], after the structures were optimized with Wien2k [57] and the PBE functional. We mimicked the influence of the substrates by simulating bulk La_2NiO_4 using the experimental lattice constants of the thin films. The

reference calculation for the bulk uses lattice constants from Ref. 33. All calculations assume the space group I4/mmm. The internal atomic positions were relaxed until the forces were below 1mRy per Bohr radius. The tight-binding hopping and crystal field parameters have been extracted from a projection onto maximally localized Wannier orbitals [58, 59] of Ni $3d_{x^2-y^2}$ and $3d_{z^2}$ character. Matrix elements of the static ($\omega = 0$) and local screened Coulomb interaction (Hubbard U and Hund's J_H) have been estimated from calculations in the constrained random phase approximation (cRPA) [51] for entangled band-structures [60] in the Wannier basis [59] using $6 \times 6 \times 6$ reducible momentum-points in the Brillouin zone.

Data availability

The data that support the findings of this study are available from the corresponding author upon reasonable request.

Author contributions

I.B. and L.M. have contributed equally to this work. G.D.L., C.B.E., A.D., and M.G. grew and characterized the La_2NiO_4 films. I.B., J. Choi, M.G.-F., S.A., K.-J.Z., and Q.W. carried out the RIXS experiments. I.B., L.M. and Q.W. analysed the RIXS data. P.M., J.M.T. and K.H. conceived, executed and analysed the *ab initio* calculations. I.B., Q.W. and J.C. conceived the project. All authors contributed to the writing of the manuscript.

Acknowledgements

I.B. acknowledges support from the Swiss Government Excellence Scholarship. L.M., G.D.L., M.G. and J.C. thank the Swiss National Science Foundation under Projects No. 200021.188564 and PP00P2_170564. Q.W. was supported by the CUHK Research Startup Fund (Grant No. 4937150). G.D.L. acknowledges support from the UZH GRC Travel Grant. We acknowledge Diamond Light Source for providing beam time on beamline I21 under Proposal MM30189. C.B.E. acknowledges support for this research through a Vannevar Bush Faculty Fellowship (ONR N00014-20-1-2844), the Gordon and Betty Moore Foundation's EPiQS Initiative, Grant GBMF9065 and NSF through the University of Wisconsin Materials Research Science and Engineering Center (DMR-1720415). The synthesis of thin films at the University of Wisconsin-Madison was supported by the US Department of Energy (DOE), Office of Science, Office of Basic Energy Sciences (BES), under award number DE-FG02-06ER46327.

Competing interests

The authors declare that they have no competing interests.

[1] P. A. Lee, N. Nagaosa, and X.-G. Wen, Doping a mott insulator: Physics of high-temperature superconductivity, *Rev. Mod. Phys.* **78**, 17 (2006).

[2] N. B. Christensen, H. M. Rønnow, D. F. McMorrow, A. Harrison, T. G. Perring, M. Enderle, R. Coldea, L. P. Regnault, and G. Aeppli, Quantum dynamics and entanglement of spins on a square lattice, *PNAS* **104**, 15264 (2007).

[3] N. S. Headings, S. M. Hayden, R. Coldea, and T. G. Perring, Anomalous High-Energy Spin Excitations in the High- T_c Superconductor-Parent Antiferromagnet La_2CuO_4 , *Phys. Rev. Lett.* **105**, 247001 (2010).

[4] R. Coldea, S. M. Hayden, G. Aeppli, T. G. Perring, C. D. Frost, T. E. Mason, S.-W. Cheong, and Z. Fisk, Spin waves and electronic interactions in La_2CuO_4 , *Phys. Rev. Lett.* **86**, 5377 (2001).

[5] K. Choo, T. Neupert, and G. Carleo, Two-dimensional frustrated J_1-J_2 model studied with neural network quantum states, *Phys. Rev. B* **100**, 125124 (2019).

[6] L. Capriotti and S. Sorella, Spontaneous plaquette dimerization in the J_1-J_2 Heisenberg model, *Phys. Rev. Lett.* **84**, 3173 (2000).

[7] L. Capriotti, F. Becca, A. Parola, and S. Sorella, Resonating valence bond wave functions for strongly frustrated spin systems, *Phys. Rev. Lett.* **87**, 097201 (2001).

[8] G.-M. Zhang, H. Hu, and L. Yu, Valence-bond spin-liquid state in two-dimensional frustrated spin-1/2 Heisenberg antiferromagnets, *Phys. Rev. Lett.* **91**, 067201 (2003).

[9] S.-S. Gong, W. Zhu, D. N. Sheng, O. I. Motrunich, and M. P. A. Fisher, Plaquette ordered phase and quantum phase diagram in the spin- $\frac{1}{2}$ J_1-J_2 square Heisenberg model, *Phys. Rev. Lett.* **113**, 027201 (2014).

[10] O. P. Sushkov, J. Oitmaa, and Z. Weihong, Quantum phase transitions in the two-dimensional J_1-J_2 model, *Phys. Rev. B* **63**, 104420 (2001).

[11] H. C. Jiang, F. Krüger, J. E. Moore, D. N. Sheng, J. Zaanen, and Z. Y. Weng, Phase diagram of the frustrated spatially-anisotropic $S=1$ antiferromagnet on a square lattice, *Phys. Rev. B* **79**, 174409 (2009).

[12] P. W. Anderson, The Resonating Valence Bond State in La_2CuO_4 and Superconductivity, *Science* **235**, 1196 (1987).

[13] E. Dagotto and A. Moreo, Phase diagram of the frustrated spin-1/2 Heisenberg antiferromagnet in 2 dimensions, *Phys. Rev. Lett.* **63**, 2148 (1989).

[14] H. J. Schulz, T. A. Ziman, and D. Poilblanc, Magnetic order and disorder in the frustrated quantum Heisenberg antiferromagnet in two dimensions, *Journal de Physique I* **6**, 675–703 (1996).

[15] K. S. D. Beach, Master equation approach to computing rvb bond amplitudes, *Phys. Rev. B* **79**, 224431 (2009).

[16] Q. Wang, Y. Shen, B. Pan, X. Zhang, K. Ikeuchi, K. Iida, A. D. Christianson, H. C. Walker, D. T. Adroja, M. Abdel-Hafiez, X. Chen, D. A. Chareev, A. N. Vasiliev, and J. Zhao, Magnetic ground state of FeSe, *Nat. Commun.* **7**, 12182 (2016).

[17] Y. Gu, Q. Wang, H. Wo, Z. He, H. C. Walker, J. T. Park, M. Enderle, A. D. Christianson, W. Wang, and J. Zhao, Frustrated magnetic interactions in FeSe, *Phys. Rev. B* **106**, L060504 (2022).

[18] O. Mustonen, S. Vasala, E. Sadrollahi, K. P. Schmidt, C. Baines, H. C. Walker, I. Terasaki, F. J. Litterst, E. Baggio-Saitovitch, and M. Karppinen, Spin-liquid-like state in a spin-1/2 square-lattice antiferromagnet perovskite induced by $d^{10}-d^0$ cation mixing, *Nat. Commun.* **9**, 1085 (2018).

[19] L. J. P. Ament, M. van Veenendaal, T. P. Devvereaux, J. P. Hill, and J. van den Brink, Resonant inelastic x-ray scattering studies of elementary excitations, *Rev. Mod. Phys.* **83**, 705 (2011).

[20] L. Martinelli, D. Betto, K. Kummer, R. Arpaia, L. Braicovich, D. Di Castro, N. B. Brookes, M. Moretti Sala, and G. Ghiringhelli, Fractional Spin Excitations in the Infinite-Layer Cuprate CaCuO_2 , *Phys. Rev. X* **12**, 021041 (2022).

[21] Q. Wang, K. von Arx, M. Horio, D. J. Mukkattukavil, J. Küspert, Y. Sassa, T. Schmitt, A. Nag, S. Pyon, T. Takayama, H. Takagi, M. Garcia-Fernandez, K.-J. Zhou, and J. Chang, Charge order lock-in by electron-phonon coupling in $\text{La}_{1.675}\text{Eu}_{0.2}\text{Sr}_{0.125}\text{CuO}_4$, *Sci. Adv.* **7**, eabg7394 (2021).

[22] O. Ivashko, M. Horio, W. Wan, N. B. Christensen, D. E. McNally, E. Paris, Y. Tseng, N. E. Shaik, H. M. Rønnow, H. I. Wei, C. Adamo, C. Lichtensteiger, M. Gibert, M. R. Beasley, K. M. Shen, J. M. Tomczak, T. Schmitt, and J. Chang, Strain-engineering Mott-insulating La_2CuO_4 , *Nat. Commun.* **10**, 786 (2019).

[23] J. Goodenough and S. Ramasesha, Further evidence for the coexistence of localized and itinerant 3d electrons in La_2NiO_4 , *Materials Research Bulletin* **17**, 383 (1982).

[24] P. G. Radaelli, D. G. Hinks, A. W. Mitchell, B. A. Hunter, J. L. Wagner, B. Dabrowski, K. G. Vandervoort, H. K. Viswanathan, and J. D. Jorgensen, Structural and superconducting properties of $\text{La}_{2-x}\text{Sr}_x\text{CuO}_4$ as a function of sr content, *Phys. Rev. B* **49**, 4163 (1994).

[25] A. Nag, H. C. Robarts, F. Wenzel, J. Li, H. Elnaggar, R.-P. Wang, A. C. Walters, M. García-Fernández, F. M. F. de Groot, M. W. Haverkort, and K.-J. Zhou, Many-body physics of single and double spin-flip excitations in nio, *Phys. Rev. Lett.* **124**, 067202 (2020).

[26] G. Ghiringhelli, M. Matsubara, C. Dallera, F. Fracassi, R. Gusmeroli, A. Piazzalunga, A. Tagliaferri, N. B. Brookes, A. Kotani, and L. Braicovich, NiO as a test case for high resolution resonant inelastic soft x-ray scattering, *J. Phys.: Condens. Matter* **17**, 5397 (2005).

[27] J. Q. Lin, P. Villar Arribi, G. Fabbri, A. S. Botana, D. Meyers, H. Miao, Y. Shen, D. G. Mazzone, J. Feng, S. G. Chiuzbaian, A. Nag, A. C. Walters, M. García-Fernández, K.-J. Zhou, J. Pelliciari, I. Jarrige, J. W. Freeland, J. Zhang, J. F. Mitchell, V. Bisogni, X. Liu, M. R. Norman, and M. P. M. Dean, Strong superexchange in a $d^{9-\delta}$ nickelate revealed by resonant inelastic x-ray scattering, *Phys. Rev. Lett.* **126**, 087001 (2021).

[28] G. Ghiringhelli, A. Piazzalunga, C. Dallera, T. Schmitt, V. N. Strocov, J. Schlappa, L. Patthey, X. Wang, H. Berger, and M. Grioni, Observation of Two Nondispersing Magnetic Excitations in NiO by Resonant Inelastic Soft-X-Ray Scattering, *Phys. Rev. Lett.* **102**, 027401 (2009).

[29] L. Pintschovius, J. M. Bassat, P. Odier, F. Gervais, G. Chevrier, W. Reichardt, and F. Gompf, Lattice dynamics of La_2NiO_4 , *Phys. Rev. B* **40**, 2229 (1989).

[30] L. Pintschovius, J.-M. Bassat, P. Odier, F. Gervais, B. Hennion, and W. Reichardt, Phonon Anomalies in La_2NiO_4 , *Europhysics Letters* **5**, 247 (1988).

[31] G. Fabbris, D. Meyers, L. Xu, V. M. Katukuri, L. Horzoi, X. Liu, Z.-Y. Chen, J. Okamoto, T. Schmitt, A. Uldry, B. Delley, G. D. Gu, D. Prabhakaran, A. T. Boothroyd, J. van den Brink, D. J. Huang, and M. P. M. Dean, Doping Dependence of Collective Spin and Orbital Excitations in the Spin-1 Quantum Antiferromagnet $\text{La}_{2-x}\text{Sr}_x\text{NiO}_4$ Observed by X Rays, *Phys. Rev. Lett.* **118**, 156402 (2017).

[32] K. Nakajima, K. Yamada, S. Hosoya, T. Omata, and Y. Endoh, Spin-Wave Excitations in Two Dimensional Antiferromagnet of Stoichiometric La_2NiO_4 , *Journal of the Physical Society of Japan* **62**, 4438–4448 (1993).

[33] A. N. Petsch, N. S. Headings, D. Prabhakaran, A. I. Kolesnikov, C. D. Frost, A. T. Boothroyd, R. Coldea, and S. M. Hayden, High-energy spin waves in the spin-1 square-lattice antiferromagnet La_2NiO_4 , [arXiv:2304.02546](https://arxiv.org/abs/2304.02546) (2023).

[34] Y. Y. Peng, G. Dellea, M. Minola, M. Conn, A. Amorese, D. Di Castro, G. M. De Luca, K. Kummer, M. Saluzzo, X. Sun, X. J. Zhou, G. Balestrino, M. Le Tacon, B. Keimer, L. Braicovich, N. B. Brookes, and G. Ghiringhelli, Influence of apical oxygen on the extent of in-plane exchange interaction in cuprate superconductors, *Nature Phys.* **13**, 1201–1206 (2017).

[35] O. Ivashko, N. E. Shaik, X. Lu, C. G. Fatuzzo, M. Dantz, P. G. Freeman, D. E. McNally, D. Destraz, N. B. Christensen, T. Kurosawa, N. Momono, M. Oda, C. E. Matt, C. Monney, H. M. Rønnow, T. Schmitt, and J. Chang, Damped spin excitations in a doped cuprate superconductor with orbital hybridization, *Phys. Rev. B* **95**, 214508 (2017).

[36] G. Aeppli and D. J. Buttrey, Magnetic Correlations in $\text{La}_2\text{NiO}_{4+\delta}$, *Phys. Rev. Lett.* **61**, 203 (1988).

[37] K. Yamada, T. Omata, K. Nakajima, S. Hosoya, T. Sumida, and Y. Endoh, Magnetic structure and weak ferromagnetism of $\text{La}_2\text{NiO}_{4+\delta}$, *Physica C: Superconductivity* **191**, 15 (1992).

[38] J. Rodriguez-Carvajal, M. T. Fernandez-Diaz, and J. L. Martinez, Neutron diffraction study on structural and magnetic properties of La_2NiO_4 , *J. Phys.: Condens. Matter* **3**, 3215 (1991).

[39] K. Yamada, M. Arai, Y. Endoh, S. Hosoya, K. Nakajima, T. Perring, and A. Taylor, Complete Two-Dimensional Antiferromagnetic Spin-Wave Dispersion Relation of La_2NiO_4 Determined by Chopper Spectrometer Installed at the Pulsed Neutron Source, *J. Phys. Soc. Jpn.* **60**, 1197 (1991).

[40] J. Igarashi, $1/S$ expansion for thermodynamic quantities in a two-dimensional Heisenberg antiferromagnet at zero temperature, *Phys. Rev. B* **46**, 10763 (1992).

[41] H. Lu, M. Rossi, A. Nag, M. Osada, D. F. Li, K. Lee, B. Y. Wang, M. Garcia-Fernandez, S. Agrestini, Z. X. Shen, E. M. Been, B. Moritz, T. P. Devoreaux, J. Zaanen, H. Y. Hwang, K.-J. Zhou, and W. S. Lee, Magnetic excitations in infinite-layer nickelates, *Science* **373**, 213 (2021).

[42] Q. Gao, S. Fan, Q. Wang, J. Li, X. Ren, I. Bialo, A. Drewanowski, P. Rothenbühler, J. Choi, Y. Wang, T. Xiang, J. Hu, K.-J. Zhou, V. Bisogni, R. Comin, J. Chang, J. Pelliciari, X. J. Zhou, and Z. Zhu, Magnetic Excitations in Strained Infinite-layer Nickelate PrNiO_2 , [arXiv:2208.05614](https://arxiv.org/abs/2208.05614) (2022).

[43] J.-Y. P. Delannoy, M. J. P. Gingras, P. C. W. Holdsworth, and A.-M. S. Tremblay, Low-energy theory of the $t - t' - t'' - U$ Hubbard model at half-filling: Interaction strengths in cuprate superconductors and an effective spin-only description of La_2CuO_4 , *Phys. Rev. B* **79**, 235130 (2009).

[44] B. Dalla Piazza, M. Mourigal, M. Guarise, H. Berger, T. Schmitt, K. J. Zhou, M. Grioni, and H. M. Rønnow, Unified one-band hubbard model for magnetic and electronic spectra of the parent compounds of cuprate superconductors, *Phys. Rev. B* **85**, 100508 (2012).

[45] M. Horio, C. E. Matt, K. Kramer, D. Sutter, A. M. Cook, Y. Sassa, K. Hauser, M. Månssson, N. C. Plumb, M. Shi, O. J. Lipscombe, S. M. Hayden, T. Neupert, and J. Chang, Two-dimensional type-II Dirac fermions in layered oxides, *Nat. Commun.* **9**, 3252 (2018).

[46] M. Uchida, K. Ishizaka, P. Hansmann, X. Yang, M. Sakano, J. Miyawaki, R. Arita, Y. Kaneko, Y. Takata, M. Oura, A. Toschi, K. Held, A. Chainani, O. K. Andersen, S. Shin, and Y. Tokura, Orbital characters of three-dimensional Fermi surfaces in $\text{Eu}_{2-x}\text{Sr}_x\text{NiO}_4$ as probed by soft-x-ray angle-resolved photoemission spectroscopy, *Phys. Rev. B* **84**, 241109 (2011).

[47] M. Uchida, K. Ishizaka, P. Hansmann, Y. Kaneko, Y. Ishida, X. Yang, R. Kumai, A. Toschi, Y. Onose, R. Arita, K. Held, O. K. Andersen, S. Shin, and Y. Tokura, Pseudogap of Metallic Layered Nickelate $R_{2-x}\text{Sr}_x\text{NiO}_4$ ($R = \text{Nd, Eu}$) Crystals Measured Using Angle-Resolved Photoemission Spectroscopy, *Phys. Rev. Lett.* **106**, 027001 (2011).

[48] C. E. Matt, D. Sutter, A. M. Cook, Y. Sassa, M. Månssson, O. Tjernberg, L. Das, M. Horio, D. Destraz, C. G. Fatuzzo, K. Hauser, M. Shi, M. Kobayashi, V. N. Strocov, T. Schmitt, P. Dudin, M. Hoesch, S. Pyon, T. Takayama, H. Takagi, O. J. Lipscombe, S. M. Hayden, T. Kurosawa, N. Momono, M. Oda, T. Neupert, and J. Chang, Direct observation of orbital hybridisation in a cuprate superconductor, *Nat. Commun.* **9**, 972 (2018).

[49] J. M. Tomczak, T. Miyake, R. Sakuma, and F. Aryasetiawan, Effective Coulomb interactions in solids under pressure, *Phys. Rev. B* **79**, 235133 (2009).

[50] R. Lemanski and J. Matysiak, Two-orbital Hubbard model vs spin $S = 1$ Heisenberg model: Studies on clusters, *Condensed Matter Physics* **21**, 33301 (2018).

[51] F. Aryasetiawan, M. Imada, A. Georges, G. Kotliar, S. Biermann, and A. I. Lichtenstein, Frequency-dependent local interactions and low-energy effective models from electronic structure calculations, *Phys. Rev. B* **70**, 195104 (2004).

[52] A. H. MacDonald, S. M. Girvin, and D. Yoshioka, Reply to “Comment on ‘ t/U expansion for the Hubbard model’”, *Phys. Rev. B* **41**, 2565 (1990).

[53] J. P. Podkaminer, J. J. Patzner, B. A. Davidson, and C. B. Eom, Real-time and *in situ* monitoring of sputter deposition with RHEED for atomic layer controlled growth, *APL Materials* **4**, 086111 (2016).

[54] K.-J. Zhou, A. Walters, M. Garcia-Fernandez, T. Rice, M. Hand, A. Nag, J. Li, S. Agrestini, P. Garland, H. Wang, S. Alcock, I. Nistea, B. Nutter, N. Rubies, G. Knap, M. Gaughran, F. Yuan, P. Chang, J. Emmins, and G. Howell, I21: an advanced high-resolution resonant inelastic X-ray scattering beamline at Diamond

Light Source, *J. Synchrotron Rad.* **29**, 563 (2022).

[55] S. Toth and B. Lake, Linear spin wave theory for single-Q incommensurate magnetic structures, *Journal of Physics: Condensed Matter* **27**, 166002 (2015).

[56] M. Methfessel, M. van Schilfgaarde, and R. Casali, A full-potential lmto method based on smooth hankel functions, in *Electronic Structure and Physical Properties of Solids: The Uses of the LMTO Method, Lecture Notes in Physics*. H. Dreysse, ed. **535** (2000).

[57] P. Blaha, K. Schwarz, F. Tran, R. Laskowski, G. K. H. Madsen, and L. D. Marks, WIEN2k: An APW+lo program for calculating the properties of solids, *J. Chem. Phys.* **152**, 074101 (2020).

[58] N. Marzari, A. A. Mostofi, J. R. Yates, I. Souza, and D. Vanderbilt, Maximally localized Wannier functions: Theory and applications, *Rev. Mod. Phys.* **84**, 1419 (2012).

[59] T. Miyake and F. Aryasetiawan, Screened Coulomb interaction in the maximally localized Wannier basis, *Phys. Rev. B* **77**, 085122 (2008).

[60] T. Miyake, F. Aryasetiawan, and M. Imada, *Ab initio* procedure for constructing effective models of correlated materials with entangled band structure, *Phys. Rev. B* **80**, 155134 (2009).